Konrad-Zuse-Zentrum für Informationstechnik Berlin

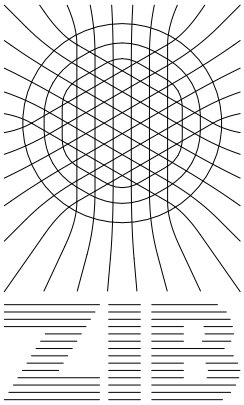

Dynamics of Erbium–doped Waveguide Lasers: Modelling, Reliable Simulation, and Comparison with Experiments

Ch. Schütte*+, M. Dinand#, G. Zumbusch*, R. Brinkmann#

* Konrad–Zuse–Zentrum für Informationstechnologie, Berlin (ZIB)
Heilbronner Str. 10, D–10711 Berlin–Wilmersdorf, Germany
schuette@zib–berlin.de

Angewandte Physik, Universität–GH Paderborn
Warburger Str. 100, D–33098 Paderborn, Germany
sol_md@physik.uni–paderborn.de

+ Institut für Mathematik I, Freie Universität Berlin
Arnimallee 6, D–14195 Berlin, Germany

SC 95-19 (August 1995)

Dynamics of Erbium–doped Waveguide Lasers: Modelling, Reliable Simulation, and Comparison with Experiments

Ch. Schütte, M. Dinand, G. Zumbusch, R. Brinkmann

October 9, 1995

Abstract

A theoretical investigation of the dynamic properties of integrated optical Er–doped waveguide lasers is presented. It includes the construction of a physical model and of numerical techniques which allow reliable simulations of the dynamical behaviour of the laser signal depending on essential parameters of the laser device and on its external, time–dependent pump radiation. Therefore, a physical theory is developed which describes the propagation of light and its interaction with the active substrate in the laser cavity. This is realized in two steps. First, a *fundamental model* based on Maxwell's equations and on rate equations for the transitions in the active medium is constructed. Since this turns out to prohibit reliable simulations, it is, in a second step, reformulated via averaging in time and space which suppresses the fluctuations on the fastest time scales but represents them correctly. For this *reduced model* reliable and efficient simulation techniques using adaptive control schemes are designed and implemented. We apply the linear–implicit Euler discretization with extrapolation in time and a multilevel quadrature scheme in space. Finally, the model is justified in comparison with experimental observations in four cases of technological relevance.

Keywords: modelling, waveguide laser, reliable simulations, adaptivity

Contents

1 Introduction

In parallel with the successful development of erbium–doped fiber amplifiers and lasers [1, 2, 3], which revolutionized the field of optical communications [4, 5], there has been a growing interest in erbium–doped planar devices during the last years [6, 7, 8, 9]. The ability to generate, guide, amplify, filter and modulate light on the same integrated optical chip opens the possibility to simultaneously combine active and passive components and therefore to develop different kinds of multifunctional lossless/amplifying devices and a new class of integrated optical lasers with promising applications in future technologies. Due to the increasing complexity of such devices the requirements in the fabrication technology increase; experimental investigations become costly and time–consuming. Therefore, the need for theoretical modelling for the analysis of these devices is obvious. Quantitative but also qualitative modelling is an important tool to improve single components as well as fully integrated chips, to shorten the development time by simultaneously reducing the development costs and therefore to accelerate the commercial use of these devices. Furthermore, theoretical modelling gives a better understanding of the physical processes involved, because it allows the determination of characteristic properties of the devices as functions of different technical parameters.

The objective of this paper is to describe the interplay between modelling and simulation concerning the theoretical investigation of the dynamic properties of integrated optical Er–doped waveguide lasers. It is a typical example for the cooperation of computational science and scientific computing in the context of development of a particular technology. The text is written with the intention that it should be understandable for both, physicist and numerical mathematician, and that it should summarize the main steps, drawbacks, and results, but also benefits and problems of the interdisciplinary cooperation in the presented case.

Fig. 1 schematically shows a waveguide laser. The basic structure is a locally erbium–doped waveguide with an erbium–concentration profile depending on the lateral coordinates x and y. These waveguides can be used as optical amplifiers or in combination with feedback elements (mirrors) on the endfaces as waveguide lasers. Depending on the waveguide fabrication process, modes with different spatial distributions and certain wavelengths propagate through the waveguide leading to light/matter–interaction with the active ions. Therefore, one has to model the time–dependent population densities of the energy levels of the erbium–ions involved (indicated in the upper left diagram) and the evolution of the

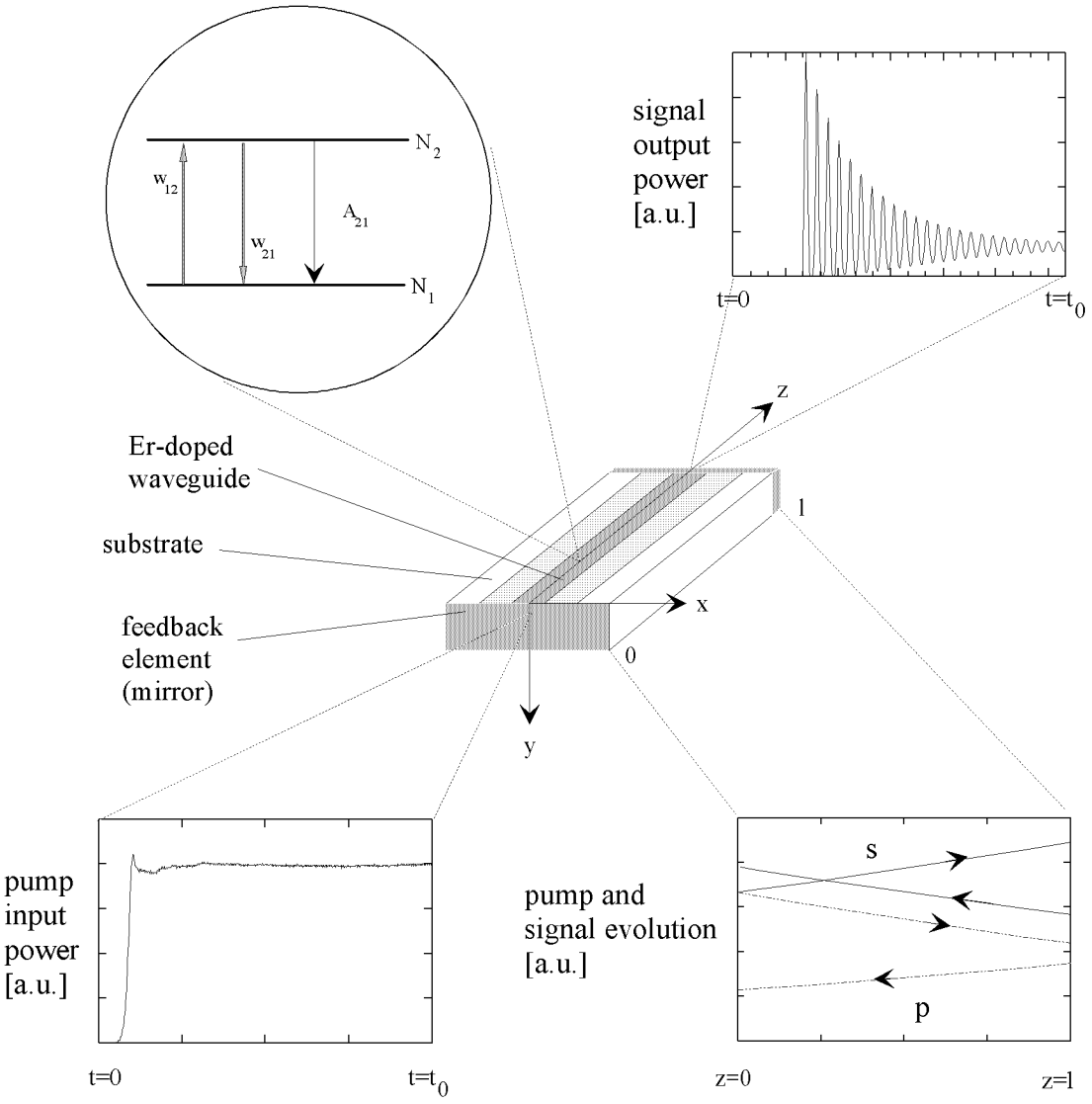

Fig. 1: Locally erbium–doped waveguide laser of length l. x (y) describes the horizontal (vertical) direction of the waveguide cross section, z is the propagation direction. In order to describe the light matter interaction causing optical amplification one has to model the dynamics of the corresponding population densities ($N_i, i = 1, 2$ with $N_0 = N_1 + N_2$) of the erbium–ions involved (upper left diagram (the terms w_{12}, w_{21} and A_{21} will be explained in the text)) and the evolution of the pump and the signal mode intensities along the propagation direction (lower right diagram). Especially the signal output power (upper right diagram) as function of a time–dependent pump input power (lower left diagram) is of particular interest.

guided modes in the waveguide taking into account the reflection of these waves at the waveguide endfaces (sketched schematically in the lower right diagram). The excitation of the active ions is determined by the external, time–dependent pump radiation (see the lower left diagram), which is coupled into the waveguide at one of the endfaces (longitudinal pumping). If sufficient pump power is provided, population inversion (the upper laser level population exceeds the population of the lower laser level) will be achieved. Then, amplification due to stimulated emission and therefore, laser operation starts (upper right diagram).

It meets universal acceptance that a fundamental model for the description of these processes must be based on Maxwell's equations including material laws describing the interaction between light and the Er–atoms in the substrate. However, this interaction can be seen as a small perturbation of the light propagation properties of the unperturbed waveguide (without Er–doping). The pure waveguide is characterized by its eigenmodes. Thus, the fundamental model can be formulated in terms of the interaction of these eigenmodes. A first modelling step based on this approach is worked out in section 2 and results in a mathematical problem including coupled partial differential equations (PDEs) with reflection boundary conditions.

For devices of practical interest this problem unfortunately is numerically intractable, i.e. the computational effort for a reliable simulation is too large even for the fastest computers (cf. section 2.2). Therefore, section 3 presents a reformulation of the model via averaging in time and space which finally leads to an initial value problem (IVP) which now can be treated numerically. In terms of numerical classification this problem is "stiff", i.e. its reliable and efficient integration requires the application of implicit discretizations. Furthermore, the spatial part of the original problem includes integrals which depend on the solution and must be evaluated in each time step. Section 4 explains how time and space discretization can be realized efficiently by using adaptive control schemes which automatically minimize the computational effort by adapting space–discretization and stepsizes in time to the properties of the solution.

We want to emphasize that in our understanding "modelling steps" need not be justified by mathematical *proofs* but by the *usefulness* of the resulting model with respect to comparison with experimental observations. Thus, our model results from physical construction and reformulation, not from mathematical deduction. After the formulation of the final model equations in section 3, the domain of physics is left and purely mathematical arguments are used in section 4. In section 5, usefulness of the model is

discussed via comparison of simulation with experimental observation, considering four different dynamical processes all of them being of practical importance. All the calculations presented in this section have been particularly performed for titanium–diffused erbium–doped lithium–niobate (Ti:Er:$LiNbO_3$) waveguide lasers [8, 9].

2 Basic Model

In this section the fundamental equations for the theoretical modelling of longitudinally pumped locally erbium–doped waveguide lasers are presented. The model is based on equations for the pump and signal evolution through the doped waveguide along the propagation direction, which can be derived from Maxwell's equations (using a semiclassical approach for the determination of the atomic susceptibility tensor) and on time– and space–dependent rate equations describing the population dynamics of the energy levels of the erbium ions involved. The combination with initial and boundary conditions leads to a full description of the light matter interaction causing optical amplification and laser operation.

Equation of Continuity:

The propagation of electromagnetic waves in free space is modelled with space– (r) and time–dependent (t) electric ($E(r,t)$) and magnetic ($H(r,t)$) field vectors. In a medium two more vector fields have to be considered: the dielectric displacement ($D(r,t)$) and the magnetic flux density ($B(r,t)$). The interaction between the vector fields itself and the medium, in which they propagate, can be described with Maxwell's theory and specific material equations. For a dielectric, linear, inhomogeneous material, which is free of electric charges ($\rho(r,t)=0$) and currents ($j(r,t)=0$) Maxwell's equations relate the four fields E, D, B and H by [10]:

$$\begin{aligned} \nabla \times E &= -\partial_t B \\ \nabla \times H &= \partial_t D \\ \nabla \cdot D &= 0 \\ \nabla \cdot B &= 0. \end{aligned} \tag{1}$$

For completeness, material equations have to be added connecting the electric displacement D with the electric field E depending on the electric properties, and the magnetic flux

density B with the magnetic field H depending on the magnetic properties of the medium:

$$B = B(H) \qquad \text{and} \qquad D = D(E). \tag{2}$$

For linear materials these equations are canonically given using the amplitudes $\widehat{A}(\cdot,\omega)$ of the "elementary waves" $\exp(i\omega t)$, i.e. via the wavepacket ansatz

$$A(r,t) = \int_{-\infty}^{\infty} \widehat{A}(r,\omega,t) e^{i\omega t} d\omega \qquad A = E, D, B, H \tag{3}$$

for the field vectors. In our case they read

$$\begin{aligned} \widehat{B}(r,\omega,t) &= \widehat{\mu}(r,\omega,t)\ \widehat{H}(r,\omega,t) \\ \widehat{D}(r,\omega,t) &= \widehat{\epsilon}(r,\omega,t)\ \widehat{E}(r,\omega,t); \end{aligned} \tag{4}$$

the amplitudes $\widehat{A}(r,\omega,t)$ are explicitly time–dependent via the time–dependency of the permeability and the susceptibility tensors, $\widehat{\mu}(r,\omega,t)$ and $\widehat{\epsilon}(r,\omega,t)$. In the following we restrict our discussion to nonmagnetic materials – then, $\widehat{\mu}$ can be replaced by the constant vacuum permeability tensor $\widehat{\mu}_0 \cdot 1$ — and to dielectric materials, in which the dielectric tensor $\widehat{\epsilon}$ can be expressed as:

$$\widehat{\epsilon}(r,\omega,t) = \epsilon(x,y,\omega) + \Delta\epsilon(r,\omega,t). \tag{5}$$

The term $\Delta\epsilon$ represents a small space– and time–dependent perturbation of the stationary dielectric susceptibility tensor ϵ, which itself contains the waveguide properties. $\Delta\epsilon$ results from the time–dependent interaction between the propagating light and the active ions (see Fig. 1). Starting with (1), taking into account (3) and (5), neglecting the term $(\nabla \cdot \widehat{E}) = -(1/\widehat{\epsilon})\nabla\widehat{\epsilon} \cdot \widehat{E}$ under the assumption that $\widehat{\epsilon}$ does not vary significantly within a wavelength distance and, furthermore, using first order approximations (with respect to $\Delta\epsilon$ and $\partial_t \widehat{E}$ being small) the following wave equation can be derived [11]:

$$\nabla^2 \widehat{E} + \mu_0 \omega^2 \epsilon \widehat{E} = \mu_0 \omega \left(2i\epsilon\partial_t - \omega\Delta\epsilon\right) \widehat{E}. \tag{6}$$

Analog assumptions result in a similar equation for $\widehat{H}$.

The principal strategy for solving (6) is to transform it using an eigenfunction expansion with respect to the *unperturbed wave equation* ($\Delta\epsilon = 0$)

$$\nabla^2 \widehat{E}_0 + \mu_0 \omega^2 \epsilon \widehat{E}_0 = 0 \tag{7}$$

for $\widehat{E}_0 = \widehat{E}_0(x,y,\omega)$, which, as well as ϵ, is *not* explicitly time–dependent ($\partial_t \widehat{E}_0 = 0$). By splitting $\widehat{E}_0$ into transversal and longitudinal components ($\widehat{E}_0 = \mathcal{E}_t + \mathcal{E}_z$) and using (1), it can be shown that the longitudinal components can be written as function of the transversal components. Therefore, we concentrate our further discussion on the transversal components only. Then, using the product ansatz $\widehat{E}_0 = \mathcal{E}_t e^{-i\beta z}$, the wave equation (7) can be reduced to an eigenvalue problem for $\mathcal{E}_t$:

$$\left(\partial_x^2 + \partial_y^2 + \mu_0\omega^2\epsilon - \beta^2\right)\mathcal{E}_t = 0. \tag{8}$$

The corresponding eigenfunctions $(\mathcal{E}_{t,m}, \mathcal{H}_{t,m})$ are called the "eigenmodes" of the waveguide. The eigenvalues β_m are either discrete (guided modes) or continuous (radiation modes) [12]. All the modes, guided and radiation modes, are orthogonal to each other, and build an orthogonal basis in the appropriate function space [13]. It is convenient to normalize the modal fields to the total power P of the system. We neglect the radiation modes, i.e. we restrict the propagation to the subspace spanned by the guided modes (Galerkin approximation). In this subspace the orthogonal relation can be written as:

$$\int \left(\mathcal{E}_{t,m} \times \mathcal{H}_{t,l}^*\right)_z \, dx\, dy = 2P\,\mathrm{sgn}(\beta_m)\,\delta_{ml}. \tag{9}$$

An arbitrary field distribution can be expressed as a linear combination (superposition) of the eigenmodes (eigenfunction expansion):

$$\widehat{E}(r,\omega,t) = \sum_m E_m(z,t)\,\mathcal{E}_{t,m}(x,y,\omega)\,e^{-i\beta_m z}. \tag{10}$$

Inserting this expression into (6), taking into account the orthogonality relation (9), and using the so–called *slowly varying amplitude approximation* (cf. [14]), the following system of partial differential equations for $E(z,t)$ can be derived:

$$\begin{aligned} \left(\frac{\partial}{\partial z} + \frac{1}{c_n}\frac{\partial}{\partial t}\right) E_l &= -i\sum_m K_{ml} E_m\, e^{i(\beta_l - \beta_m)z} \\ & K_{ml}(z,\omega,t) = \mathrm{sgn}(\beta_l)\frac{\omega}{4P}\int \left(\mathcal{E}_{t,l}^*\,\Delta\epsilon\,\mathcal{E}_{t,m}\right) dx\, dy. \end{aligned} \tag{11}$$

The coupling coefficients K_{ml} are given as overlap integrals between the transversal mode distributions $\mathcal{E}_{t,m}$, $\mathcal{E}_{t,l}$ and the perturbation of the dielectric susceptibility tensor $\Delta\epsilon$. The elements of $\Delta\epsilon$ depend on the choice of the coordinate system. Transforming the system to the main axis the non diagonal elements of the tensor vanish. In this case the knowledge of just K_{ll} is sufficient. $c_n = c/n$ is the light phase velocity in a medium with refractive index n.

The term $\Delta\epsilon$ results from doping the material with active ions and is called "(complex) atomic susceptibility" [15]. For rare–earth doped materials, it can be shown that the real and the imaginary part of $\Delta\epsilon$ can be written as linear combinations of the space– and time–dependent population densities of the ground (N_1) and the first excited state (N_2) of the active ions:

$$\begin{aligned} \Delta\epsilon(r,\omega,t) &= \epsilon_0\ (\chi_a'(r,\omega,t) - i\chi_a''(r,\omega,t)) \\ \\ \chi_a{}'(r\omega,t) &= +n\frac{c}{\omega}\Big[\kappa_{21}(\omega)\ N_2(r,t) - \kappa_{12}(\omega)\ N_1(r,t)\Big] \\ \chi_a''(r,\omega,t) &= -n\frac{c}{\omega}\Big[\sigma_{21}(\omega)\ N_2(r,t) - \sigma_{12}(\omega)\ N_1(r,t)\Big]. \end{aligned} \tag{12}$$

The terms $\sigma_{12}(\omega)$ and $\sigma_{21}(\omega)$ are the wavelength dependent absorption and emission cross sections; they are proportional to the absorption and emission spectra. $\kappa_{12}(\omega)$ and $\kappa_{21}(\omega)$ are the cross section for the determination of the gain–induced dispersion. Using expression (12) equation (11) can be reduced to:

$$\begin{aligned} \left(\frac{\partial}{\partial z} + \frac{1}{c_n}\frac{\partial}{\partial t}\right) E_l &= \tfrac{1}{2}\mathrm{sgn}(\beta_l)\,(g - if)\,E_l \\ \\ g &= \frac{1}{\mathcal{P}}\int (\sigma_{21}N_2 - \sigma_{12}N_1)\,|\mathcal{E}_{t,l}|^2\ dx\,dy \\ f &= \frac{1}{\mathcal{P}}\int (\kappa_{21}N_2 - \kappa_{12}N_1)\,|\mathcal{E}_{t,l}|^2\ dx\,dy \\ & \mathcal{P} = \int |\mathcal{E}_{t,l}|^2\ dx\ dy. \end{aligned} \tag{13}$$

In this model we are only interested in the evolution of the intensity amplitudes $j = j_l = E_l \cdot E_l^* = |E_l|^2$. With the definitions $j_0 = j_{0,l} = |\mathcal{E}_{t,l}|^2$, and $\sigma_{nm,j} = \sigma_{nm}(\lambda_j)$ and with the normalization condition $\mathcal{P} = \int j_0\,dx\,dy = 1$ equation (13) transforms to

$$\left(\pm\frac{\partial}{\partial z} + \frac{1}{c_n}\frac{\partial}{\partial t}\right) j^{\pm} = \left[-\tilde{\alpha}_j + \int (\sigma_{21,j}N_2 - \sigma_{12,j}N_1)\,j_0\ dx\,dy\right] j^{\pm} + \tilde{\chi}_j, \tag{14}$$

which is known as the equation of continuity for a gain–medium [16]. Waveguide scattering losses and spontaneous emission have been taken into account phenomenologically by the terms $\tilde{\alpha}_j$ and $\tilde{\chi}_j$. The $(+)$ and $(-)$–sign represents forward $(+z)$ and backward $(-z)$–propagating waves. In optically, longitudinally pumped erbium–doped waveguide structures (14) is valid for the signal $(j = s)$ as well as for the pump mode $(j = p)$.

RATE EQUATIONS:

The space and time–dependent population densities N_1, N_2 of the corresponding energy levels of the erbium–ions involved (see (13)) are described with rate equations. Neglecting ESA (*excited state absorption* [17]), ASE (*amplified spontaneous emission* [18]) and interactions between neighbouring erbium–ions (*cooperative upconversion, ion migration* [19]) amplification and therefore laser operation for the wavelength range $1.52\,\mu\text{m} < \lambda_s < 1.62\,\mu\text{m}$ pumped at $\lambda_p = 1.48\,\mu\text{m}$ can be modelled with a quasi–two–level system [11, 20] with N_1 being the population density of the ground level and N_2 that of the first excited level (both levels are split into multiple substates due to the Stark–effect). Using the notation of [21] the dynamics of the population densities N_1 and N_2 can be written as:

$$\frac{dN_1}{dt} = -\frac{dN_2}{dt} = -(R_{12} + W_{12})N_1 + (A_{21} + R_{21} + W_{21})N_2. \tag{15}$$

Defining the inversion $N = N_2 - N_1$ and the total erbium concentration $N_0 = N_2 + N_1$, an ordinary differential equation for $N(r,t)$ can be derived:

$$\begin{aligned} \frac{dN}{dt} &= (R_{12} - R_{21} + W_{12} - W_{21} - A_{21})N_0 \\ &- (R_{12} + R_{21} + W_{12} + W_{21} + A_{21})N. \end{aligned} \tag{16}$$

The (polarization dependent) transition rates R and W of the pump ($j = p$) and the signal ($j = s$) are proportional to the intensity distributions I_j, which itself can be split into three terms (the launched pump power P_j^0, the transversal mode distributions $j_0(x,y,\lambda)$ and the amplitudes $j(z,t) = j^+(z,t) + j^-(z,t)$), and to the cross sections $\sigma_{nm,j}$:

$$U_{nm} = \frac{\sigma_{nm,j}\, I_j}{h\nu_j} = \frac{\sigma_{nm,j}}{hc}\, \lambda_j\, P_j^0\, j_0(x,y,\lambda)\, j(z,t) \tag{17}$$

with $U = R, W$, $nm = 12, 21$, $j = p, s$ and h being Planck's constant. The term A_{21} describes the spontaneous transition rate which is $A_{21} = \frac{1}{\tau_{21}}$ with τ_{21} being the fluorescence lifetime of the upper laser level.

BOUNDARY CONDITIONS:

The equations for the pump and the signal intensity amplitudes (14) build a system of partial differential equations which is coupled to an ordinary differential equation (16) for the inversion. In order to model the properties of waveguide lasers (as sketched in Fig. 1)

simultaneously boundary conditions have to be fulfilled at $z = 0$ and $z = l$ resulting from the reflection of the forward and backward running modes at the feedback elements [21]:

$$\begin{aligned} j^+(0,t) &= R_1^j\, j^-(0,t) + \delta_{jp}\,(1 - R_1^j)\; P^0 \eta_j \\ j^-(l,t) &= R_2^j\, j^+(l,t) \\ & \quad j = p, s. \end{aligned} \tag{18}$$

$R_1^j = R_1(\lambda_j)$ and $R_2^j = R_2(\lambda_j)$ are the reflectivities of the front and the rear mirror for the wavelength λ_j, respectively, η_j the coupling efficiency and P^0 the normalized incident pump power within the laser cavity: $P^0 = P_{p,ex}(t)/P_p^0$ with $P_{p,ex}$ being the time–dependent external pump power and P_p^0 the launched pump power.

2.1 Set of Basic Equations

For the following discussion the basic equations (14) and (16) are abbreviated as follows:

$$\begin{aligned} \left(\frac{\partial}{\partial z} + \frac{1}{c_n}\frac{\partial}{\partial t}\right) j &= g(N)\, j \;+\; \tilde{\chi}_j \\ \frac{d}{dt} N &= \alpha(j) \;+\; \beta(j)\, N \end{aligned} \tag{19}$$

with

$$\begin{aligned} \left(\frac{\partial}{\partial z} + \frac{1}{c_n}\frac{\partial}{\partial t}\right) j &:= (A_+ p^+, A_- p^-, A_+ s^+, A_- s^-) \\ g(N) &:= -\operatorname{diag}\left(g_p(N), g_p(N), g_s(N), g_s(N)\right) \\ j &:= (p^+, p^-, s^+, s^-) \\ A_\pm &:= \left(\pm\frac{\partial}{\partial z} + \frac{1}{c_n}\frac{\partial}{\partial t}\right) \\ \tilde{\chi}_j &:= (\tilde{\chi}_p, \tilde{\chi}_p, \tilde{\chi}_s, \tilde{\chi}_s) \end{aligned} \tag{20}$$

Note, that additionally the set of initial values and the boundary conditions (18) has to be considered in order to obtain a complete model.

2.2 Numerical Intractability

Up to now, there is no explicit analytical solution of (19) available, in particular none for nontrivial parameter sets, initial, and boundary data. Thus, one is interested in an efficient and reliable numerical solution of (19). But unfortunately, (19) is intractable

even with help of numerical means. Let us briefly go into some details for explaining this surprising statement. The equation of continuity $(\partial_z + \partial_t/c_n)j = g(N)j + \tilde{\chi}_j$ for the pump and signal amplitudes j describes the transport of z–variations in $j(x, y, z, t)$ along the z–axis in time. This implies that, as long as $\partial_z j^{\pm}$ does not vanish globally in $[0, l]$, variations in j are running through the waveguide structure with velocity c_n along the z–axis being reflected at the mirrors again and again. They are simultaneously amplified or damped by their interaction with the erbium ions and by losses. This means that the smallest time scale of the dynamical behaviour described by (19) lies below the round trip time

$$\tau \;:=\; \frac{2l}{c_n} \;=\; \frac{2l\,n}{c}. \tag{21}$$

which in typical devices (with device lengths in the order of cm) approximately is $\tau \approx 1\,\mathrm{ns}$. Unfortunately, many questions of practical interest require simulation calculations on a time interval $[0, T]$ with a duration T in the range of milliseconds (cf. section 5). Thus, for solving (19) as it is, any numerical algorithm has to perform

$$\frac{T}{\tau} \;\gg\; 10^6 \tag{22}$$

time steps *at least*! Moreover, these are time steps for a BVP (boundary value problem) based on a partial differential equation. Thus, in each single time step an additional spatial problem and a large nonlinear system (required for the boundary conditions) have to be solved. Thus, the computational effort of reliable simulation calculations is much too large, even for the fastest computers available today. And, worse, even if we would be able to realize these calculations, we have to expect that the amplification of unavoidable numerical errors destroys any useful information because of the tremendous number of time steps.

3 Reformulated Model

We have seen that our basic equations are numerically not tractable, because the space and time scales of the variation of their solution are too small or rather to short. In order to make simulation calculations possible we should try to compute the "essential dynamics" only, i.e. to avoid the evaluation of all oscillatory details (forward and backward running wave fronts in the cavity). Therefore, we define "essential dynamics" via averaging and reformulate the model equations (19).

Why do we call this a *reformulation*? A first physical model has still been presented and the next step is done only because of the numerical intractability named. A mathematician would like to fix the first model trying to construct a purely mathematical *deduction* of a reduced model which then should be numerically tractable. In contrast, a physicist would use modelling arguments (additional physical assumptions, neglect of small terms, ...) aiming at the same. The next subsection is organized according to the mathematical approach, nevertheless it is *not* a deduction. But it needs two additional modelling assumptions only, which, in addition, can be separated well, are deeply mathematical, and appear in many similar situations, thus being *structural*. Because of these facts we call it a reformulation.

3.1 Averaged Dynamics

Let the *average dynamics* of a function $u = u(x,y,z,t)$ be defined with respect to the following averaging operators:

$$\begin{aligned} (\mathcal{A}_t u)(x,y,z,t) &:= \int_{-\infty}^{\infty} w_\tau(t-t')\; u(x,y,z,t')\; dt' \\ (\mathcal{A}_z u)(x,y,t) &:= \frac{1}{l}\int_0^l u(x,y,z',t)\; dz' \\ \mathcal{A} &:= \mathcal{A}_z\,\mathcal{A}_t, \end{aligned} \tag{23}$$

where w_τ is a filter kernel which makes $\mathcal{A}$ and $\mathcal{A}_t$ low pass filters with cut–off frequency $2\pi/\tau$, "smoothing" all variations on time scales below the round–trip time $\tau = 2l/c_n$. Now, if (j,N) is the exact solution of (19), we *directly* intent to compute

$$(\bar{j},\bar{N}) \;=\; (\mathcal{A}j, \mathcal{A}N)\,. \tag{24}$$

Thus, we have to operate with $\mathcal{A}$ on (19) in order to construct equations of motion for the averaged quantities $(\bar{j},\bar{N})$ only. But this leads to a fundamental problem of averaging: The right hand side of (19), i.e.

$$h(j,N) \;=\; \begin{pmatrix} g(N)\,j \,+\, \tilde{\chi}_j \\ \alpha(j) \,+\, \beta(j)\,N \end{pmatrix}, \tag{25}$$

is nonlinear and we cannot derive an equation in closed form because of the general noncommutativities

$$\mathcal{A}\,(\beta(j)\,N) \;\;\neq\;\; \beta\,(\mathcal{A}j)\;\;\mathcal{A}N$$

$$\mathcal{A}\,(g(N)\;j) \quad \neq \quad g\,(\mathcal{A}N)\;\;\mathcal{A}j.$$

This problem cannot be solved by mathematical *deduction*, i.e. in general it is not possible to construct a new function H for which $\mathcal{A}\,h(j,N) = H(\mathcal{A}j, \mathcal{A}N)$ can be *proved* mathematically! Therefore, we *remodel* (19) in order to construct equations for $(\mathcal{A}j, \mathcal{A}N)$ only. To do this, let us start with the following example–BVP

$$\left(\pm\frac{\partial}{\partial z} + \frac{1}{c_f}\frac{\partial}{\partial t}\right) f^{\pm}(z,t) = -g\;f^{\pm}(z,t) \tag{26}$$

with constant g and the boundary conditions:

$$\begin{aligned}
f^{+}(z,0) &= a e^{-gz}, && \forall z \in [0,l] && (27)\\
f^{-}(z,0) &= R_2\, a\, e^{g(z-2l)}, && \forall z \in [0,l] && (28)\\
f^{+}(0,t) &= \eta + R_1 f^{-}(0,t), && \forall t > 0 && (29)\\
f^{-}(l,t) &= R_2\, f^{+}(l,t) && \forall t > 0 && (30)
\end{aligned}$$

with a and η being constant, too. For this BVP the following theorem holds (for a proof see [21]):

THEOREM: *Let (f^{+}, f^{-}) be the solution of (26), $\xi := R_1 R_2 \exp(-2gl)$, and*

$$\kappa \;:=\; \frac{1}{l}\int_0^l (e^{-gz} \;+\; R_2\, e^{g(z-2l)})\, dz. \tag{31}$$

Then, the averaged total intensity $\bar{f} := \mathcal{A}\,(f^{+} + f^{-})$ is given by the solution of

$$\frac{1}{c_f}\frac{d}{dt}\bar{f} \quad = \quad \left(\frac{\ln(R_1R_2)}{2l} - g\right)\,\bar{f} \;-\; \frac{1}{2l}\;\frac{\ln\xi}{1-\xi}\;\kappa\,\eta \tag{32}$$

with initial value

$$\bar{f}(0) = \kappa\, a. \tag{33}$$

Moreover, for all $t > 0$ there is an $a \in R$ so that $f^{\pm}(\cdot, t)$ still fulfills conditions (27) and (28).

Our *first modelling step* is inspired by this theorem. Assume that the solution $N(x,y,z,\cdot)$ of (19) is known. Set

$$g_0 \;:=\; \mathcal{A}g(N)(t_0). \tag{34}$$

With respect to time scales below the round trip time τ, $\mathcal{A}g(N)$ is nearly a constant, i.e. we may assume that the variations in $\mathcal{A}g(N)$ are small

$$|g_0 \; - \; \mathcal{A}g(N)(t)| \; \ll \; |g_0| \qquad \forall t \in [t_0, t_0 + T] \tag{35}$$

for $T \gg \tau$. Hence, in $[t_0, t_0 + T]$, we may set $\mathcal{A}g(N) \equiv g_0$ and use the theorem given above for replacing the BVP (19) locally in time by an IVP like (32), i.e. the averaged total intensities of signal and pump

$$\bar{j} \; := \; \mathcal{A}\,(j^+ \, + \, j^-)\,, \qquad j \, = \, p, s \tag{36}$$

are given by

$$\frac{1}{c_n}\,\frac{d}{dt}\bar{j} \;\; = \;\; \left(\frac{\ln(R_1 R_2)}{2l} - \mathcal{A}g_j(N)(t_0)\right)\,\bar{j} \;\; - \;\; \frac{1}{2l}\;\frac{\ln\xi}{1-\xi}\;\kappa\,\eta, \qquad j = p, s. \tag{37}$$

In the *second modelling step* the following additional assumptions are introduced:

$$\begin{array}{rcl} \mathcal{A}g(N) & = & g(\mathcal{A}N) \\ \mathcal{A}\,(\beta(j)\,N) & = & \beta\,(\mathcal{A}j)\;\mathcal{A}N. \end{array} \tag{38}$$

With (38) we get from (19) that

$$\frac{d}{dt}\mathcal{A}N \;\; = \;\; \alpha\,(\mathcal{A}j) \;\; + \;\; \beta\,(\mathcal{A}j)\;\mathcal{A}N, \tag{39}$$

which combined with (37) leads to the following reformulation of the equations of motion (19):

$$\begin{array}{rcl} \dfrac{1}{c_n}\,\dfrac{d}{dt}\bar{j} & = & \left(\dfrac{\ln(R_1 R_2)}{2l} - g_j(\mathcal{A}N)(t)\right)\,\bar{j} \;\; - \;\; \dfrac{1}{2l}\;\dfrac{\ln\xi}{1-\xi}\;\kappa\,\eta, \qquad \bar{j} = \bar{p}, \bar{s} \\ \dfrac{d}{dt}\mathcal{A}N & = & \alpha\,(\mathcal{A}j) \;\; + \;\; \beta\,(\mathcal{A}j)\;\mathcal{A}N. \end{array} \tag{40}$$

Returning to a simpler notation by omitting the explicit reference to the averaging process ($\mathcal{A}N \to A$, $(\bar{p}, \bar{s}) \to j$), we denote this in the following form

$$\begin{array}{rcl} \dfrac{1}{c_n}\,\dfrac{d}{dt}j & = & \tilde{g}(N)\,j \;\; + \;\; \tilde{\chi}_j \\ \dfrac{d}{dt}N & = & \alpha(j) \;\; + \;\; \beta(j)\,N \end{array} \tag{41}$$

with $\tilde{g}(N) := (\ln(R_1^p R_2^p)/2l - g_p(N), \ln(R_1^s R_2^s)/2l - g_s(N))$.

3.2 Numerical Classification

The problem given by equation (41) defines an initial value problem. It is an ordinary differential equation (ODE) for s, p and $N(x, y, \cdot)$ in time which is non–linear and stiff. The property "stiffness", widely discussed in numerical mathematics [22], can be characterized by the failure of explicit "standard solvers". The iteration of an explicit discretization either leaves its stability domain and completely deviates from the solution, or the stepsizes have to be chosen so small that the algorithm is not efficient compared to integrators specialized to stiff integration problems. Therefore, an "A–stable" [22], i.e. necessarily implicit, discretization has to be chosen; details of an efficient choice are given in section 4.

The evolution of $N(x, y, \cdot)$ is defined by a linear ODE (see (41)). It can be considered as a family of single ODEs with parameter space (x, y). The members of this family are spatially decoupled with different coefficients $\alpha(x, y, \cdot)$ and $\beta(x, y, \cdot)$ for each point (x, y).

For completeness we need to know the initial values $s(0)$ and $p(0)$ and the distribution $N(x, y, 0)$ at time $t = 0$. The ODEs combined with these initial values determine a unique set of trajectories $s(t)$, $p(t)$ and $N(x, y, t)$. While the fundamental model was an initial–boundary–value problem with space–boundary conditions for solutions in space–time, the reformulation replaces these boundary conditions. We do not consider partial differential equations, but a family of ordinary differential equations.

4 Numerical Solution of the Reformulated Model

Considering the numerical solution of the well posed initial value problem we employ a state–of–the–art adaptive time–integrator for the ODE. In addition, we treat the space distribution of $N(x, y, \cdot)$ by means of an adaptive quadrature algorithm. Conceptually, we first discretize the problem in time only, applying a suitable adaptive time integrator (leading to a nonuniform grid in time). That means, that the remaining spatial subproblems are initially considered to be continuous and that we are able to solve them exactly. Afterwards, the continuous space is discretized independently for each time step and each space problem is solved up to the required accuracy (again leading to a nonuniform grid). This approach is similar to Rothe's method for parabolic problems, solving continuous Cauchy problems in space [23].

4.1 Linear Implicit Time Discretization

As mentioned above we are concerned with a stiff initial value problem. Hence we have to employ implicit integration schemes, which lead to the necessity of solving a system of nonlinear equations in each time step. Therefore, implicit discretizations rely on Newton's iteration and on the repeated solution of systems of linear equations. Instead of using fully implicit schemes, we use the linear–implicit Euler scheme, which for the ODE $\dot{x} = f(x,t)$ reads

$$(I - \tau J)\, x_{k+1} = x_k + \tau\,(f(x_k,t_k) - Jx_k) \quad \text{with} \quad J := Df(x_k,t_k). \tag{42}$$

This discretization requires the solution of only one system of linear equations in each time step and is shown to be stable for stiff IVPs, too [22]. In our case (see (41)) the resulting systems of linear equations are of a very special form, because the Jacobian J has a double arrow sparsity pattern:

$$J = \begin{bmatrix} * & & & * & * \\ & \ddots & & \vdots & \vdots \\ & & * & * & * \\ * & \cdots & * & * & * \\ * & \cdots & * & * & * \end{bmatrix} \tag{43}$$

Therefore, the iteration of the disretization (42) can be accelerated by improving the linear algebra. We use a special form of Gauss elimination exploiting the pattern (43) efficiently (described in detail in [24]). Then, each time step of (42) needs $\mathcal{O}(n)$ operations only with n being the number of unknowns, which is the number of quadrature points plus two (the unknown amplitudes for the signal and for the pump). Hence, in our case, the application of (42) is asymptotically as complex as applying an explicit discretization of the same order. The order of consistency of the linear–implicit Euler discretization is $p = 1$. For means of efficient integration we are interested in higher orders. The order is defined via the local discretization error. If we denote the considered discretization using the discrete evolution $x_{k+1} = \Psi^\tau x_k$ and use the phase flow Φ^t of the considered ODE (that means $x(t) = \Phi^t x_0$ is solution of the ODE with initial value x_0) then the order is $p = p(\Psi^\tau)$ iff

$$|\Phi^\tau x \;-\; \Psi^\tau x| \;=\; \mathcal{O}(\tau^{p+1}) \qquad \forall x. \tag{44}$$

A higher order integration usually delivers a higher accuracy, or in other words, for fixed accuracy larger time steps are possible. On the other hand, the computational effort

for each time step increases with increasing order. Hence, there is an optimal order of integration which minimizes the total effort (see below).

We use extrapolation [25] for automatic construction of higher order schemes out of single steps of the linear–implicit Euler discretization. The resulting schemes remain $A(\alpha)$–stable [25]. In addition the minimization of the total effort is realized by an adaptive control scheme (cf. section 4.3).

4.2 Spatial Discretization via Quadrature

Solving (41) we have to compute integrals of the form:

$$\int j_0(x,y)\; N(x,y,t)\; dxdy \quad j = p, s. \tag{45}$$

In general, the numerical computation of integrals is called "quadrature". Under some smoothness assumptions on the integrand, we can approximate the integral by a finite sum of the integrand evaluated at some grid points (x_i, y_i) times some specific weights w_i:

$$\int j_0(x,y)\; N(x,y,t)\; dxdy \approx \sum_i j_0(x_i,y_i)\; N(x_i,y_i,t)\; w_i, \quad j = p, s. \tag{46}$$

The set of grid points and weights represent a so–called quadrature formula. One simple example for such a formula is the rectangle rule with quadrature points at equidistant square grids and weights, which all are equal. The quality of the approximation (46) is again described by the "order" of the quadrature formula [26]. For higher order quadrature one can vary both quadrature points and weights. The rectangle rule for example is of order $p = 1$; we have used quadrature formula of different orders.

Fixing an appropriate quadrature rule, we only need to know the values of $N(x,y,t)$ at a fixed number of points (x_i, y_i). We can compute the evolution of each $N(x_i, y_i, t)$ by its initial value $N(x_i, y_i, 0)$ and its ODE with coefficients determined by the space position (x_i, y_i) and the values of s and p. In a post–processing step the distribution $N(x,y,t)$ can be recovered by means of interpolation in space. Hence we have reduced the number of unknowns of the system of ODEs from a continuous set to a finite set by means of the quadrature formula. Of course we introduce an additional error doing this, but we can control this error by error estimates for the quadrature.

4.3 Adaptivity

Considering the initial values and all the coefficients to be exact, we have got two different sources of error in the numerical simulation. The first error is due to time discretization, the second is the quadrature error. Both errors can be controlled using an adaptive order and stepsize control in time integration as well as an quadrature formula adapted to the integrands.

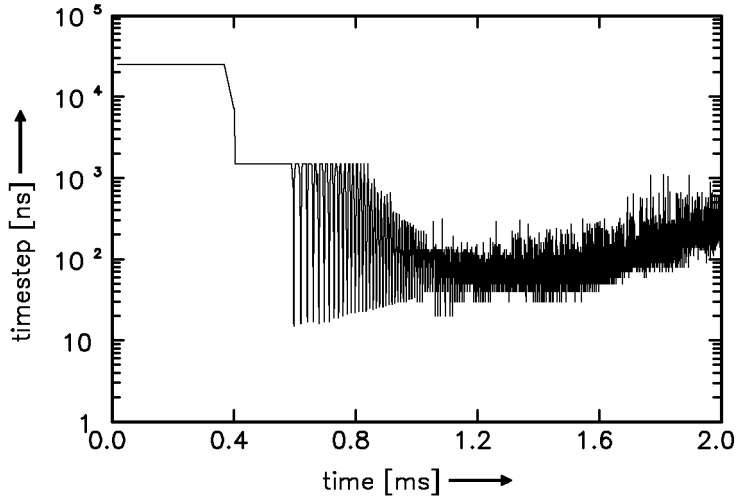

Fig. 2: Adaptive time steps of the extrapolation integrator versus time for a typical simulation of relaxation oscillations (see section 5).

We want to minimize the total work of the numerical calculation with respect to a prescribed total error tolerance. For the minimization of work of the time integration, we use large time steps wherever possible and determine the optimal order for each time step. Stepsizes and orders are chosen automatically based on error–estimates and are controlled in order to reach the prescribed error tolerance with a minimal amount of work. Let W_k be the number of operations which have to be performed for the evaluation of a time step with order $p = k$ and let τ_k be the stepsize which would be allowed with respect to the prescribed error tolerance. Then, choose that order k_{opt} for which the effort per stepsize W_k/τ_k is minimal. In the context of the linear–implicit Euler discretization and its extrapolation an automatic control scheme realizing this algorithmic idea was proposed in [27]. We use this scheme as it is implemented in the integrator EULSIM [28]. For further details see [29].

Fig. 2 shows the development of the length of the time steps during integration of (19) for a typical parameter set. It can be seen that adaptive integration is much more efficient than integration with a fixed (small) stepsize, because in the latter case the stepsize must be about the smallest stepsize occurring in Fig. 2 for realizing a comparable total error.

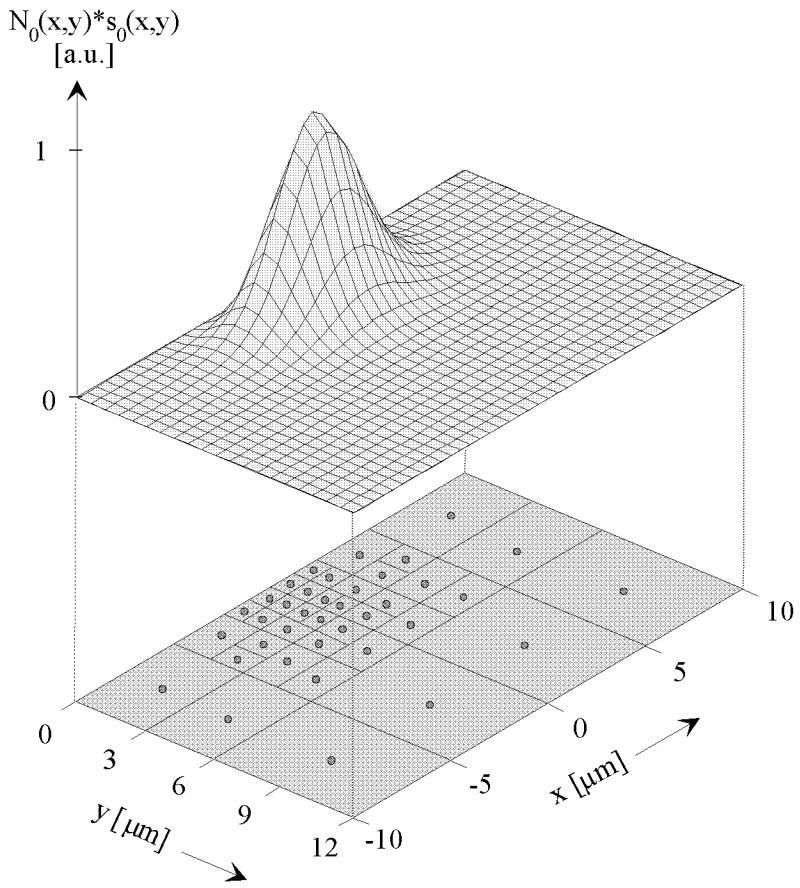

Fig. 3: Three–dimensional distribution and adaptive quadrature of $N_0(x,y) \cdot s_0(x,y)$ in space (tolerance 0.01, 19 quadrature points in one half of the domain, derived upon a one point formula).

For spatial discretization we have to select a quadrature formula which guarantees a certain error tolerance in space. In order to resolve the "details" of the integrands $(s_0 N)(x,y,\cdot)$ and $(p_0 N)(x,y,\cdot)$, we typically have to use many quadrature points near these details and only some points in (x,y)–regions where the integrands are nearly constant. It cannot be efficient to use equidistributed quadrature points with a small distance which is needed in

order to resolve the maximum of $(s_0 N)$ and $(p_0 N)$. An efficient nonuniform distribution of quadrature points is determined automatically again by employing an adaptive control scheme [30]. This adaptive procedure uses a standard quadrature formula, e.g. the rectangle rule, and starts with a rather coarse grid, e.g. with one point in the center of each of two rectangles into which the integration domain is decomposed. Then, it uses error estimates in order to decide which of these rectangles must be refined because the estimated quadrature error is too large. For each rectangle created this is iterated until the quadrature error meets the prescribed accuracy requirement (see [26]). Fig. 3 shows such an iteratively bisected domain and the corresponding distribution of the quadrature points. Due to symmetry, only one half of the domain is used for calculation. Hence the quadrature formula is constructed symmetric, too.

Using this adaptive quadrature scheme, we can reduce the number of quadrature points dramatically in comparison to the case of equidistribution. Hence we can use a small number of unknowns, speeding up the time integration and therefore the whole simulation. For example, in the situation shown in Fig. 3 our adaptive scheme needs 19 quadrature points in order to achieve the same accuracy than an uniform grid with 400 equidistributed points.

4.4 Sensitivity with Respect to Parameters

Our equations of motion (41) are nonlinear and include a lot of parameters (in the equations, in the boundary conditions, and in the initial data). Clearly, these parameters are not constants but must be determined by additional investigations either directly from experimental measurement or indirectly via theoretical modelling (further modelling steps, i.e. further approximations) [21]. Thus, we have to consider initial uncertainties ("errors") in the parameter set and the *sensitivity* of the solution with respect to these parameters, i.e. the *amplification* of these initial errors has to be taken into account. Note, that herein "amplification of errors" does not denote an effect of the numerical methods applied but an *analytical* property of the mathematical problem. Let $x = (j, N)$ be the state of our laser system and let us, for simplification of notation, write (41) in the general form $x' = f(x)$. Now, let $x(t; x_0, \Lambda)$ be the *exact solution* of this problem, denoting that the solution depends on the initial data $x(t = 0) = x_0$ and on the parameter set $\Lambda \in R^m$. In real life simulations we use a set $\Lambda = \Lambda_0$ with an upper estimate $e(0)$ for the initial error, i.e. we

know that the *proper* parameter set Λ_0' fulfills the condition:

$$\|\Lambda_0' - \Lambda_0\| \leq e(0). \tag{47}$$

Then, we are interested in the propagation of the error

$$e(t) := \max_{\|\Lambda-\Lambda_0\|\leq e(0)} \|x(t; x_0, \Lambda) - x(t; x_0, \Lambda_0)\|, \tag{48}$$

which typically increases with t. We have tested this sensitivity via numerical experiments and verified, that the increase in $e(t)$ can be dramatically. For example, the starting point of the relaxation oscillations (see section 5) is highly sensitive with respect to errors in $\tilde{\chi}_s$ (see (41)). But fortunately, these numerical experiments showed that all qualitative results are *nearly invariant* with respect to small errors (e.g. relation between starting time, decay time, and stationary state for relaxation oscillations and distance between single pulses in this case). Drawing a conclusion, already the effect of sensitivity with respect to uncertain parameters forces us to accept that the model equations do not allow an overall quantitative description of experimental observations. Nevertheless, the next section demonstrates that they are appropriate for qualitative investigations.

5 Numerical Results and Comparison with Experiments

The model constructed in the previous sections is based on different modelling steps. First, an equation of continuity for the pump and signal intensity amplitudes has been derived starting from Maxwell's equations. Together with rate equations for the population densities these equations form a BVP. Second, this has been remodelled via averaging techniques which finally leads to a reduced model consisting of an IVP only. While Maxwell's equations are generally accepted for describing light propagation correctly our reduced model has to be *justified* by successful comparison with experiments. Such justification is the objective of this section. The following three subsections will present results numerically derived from our model which qualitatively reproduce corresponding experimental observations with a specific Er–diffused Ti:$LiNbO_3$ waveguide laser. For these calculations all parameters included in the model's equations (19) have been determined experimentally (cf. [11, 21]). In the last subsection a typical example for the discussion process which arises from differences between experimental observation and simulation results is considered.

5.1 Relaxation Oscillations

Relaxation oscillations — a sequence of fairly sharp pulses in the signal output power, which after a certain time settle down to a quasi–harmonic oscillation finally producing a fairly constant output — are one of the most notable transient phenomena in solid state lasers. Typically they appear during the buildup of lasing (after switching on the pump) or as a response to different kinds of external or internal perturbances of the laser. The physical mechanism is an interplay between the pump and signal intensities within the resonator and the population densities of the active ions involved [14].

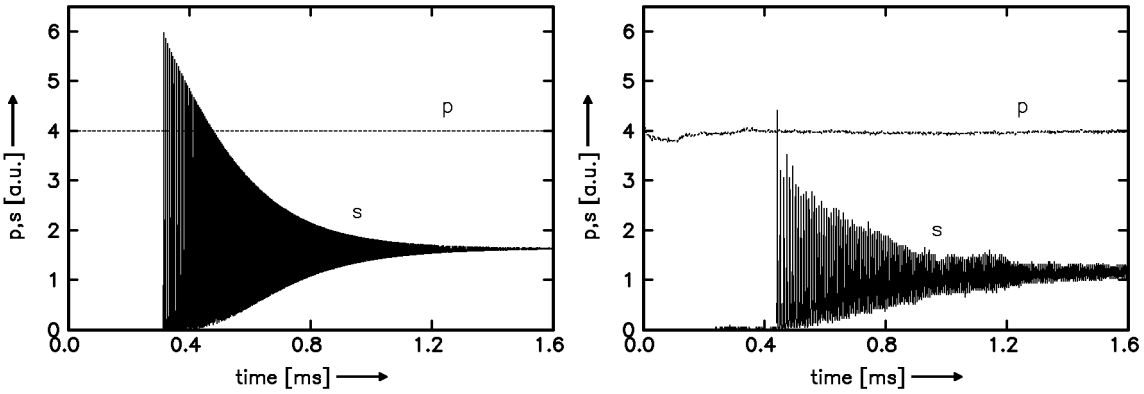

Fig. 4: Relaxation oscillations of an Er:Ti:$LiNbO_3$–waveguide laser. Left: Simulation. Right: Experimental result. The incident pump power is constant in time.

Due to its characteristic frequency and damping rate detailed investigations of the relaxation oscillations can be used for the extraction of basic laser parameters, as for instance the quality of the resonator [31]. Furthermore, they indicate the ability for the generation of short pulses. Nevertheless, in many applications relaxations oscillations, or more general, irregular fluctuations of the output power of a laser, are unwanted. An exact description and a reliable control is of particular interest.

For Er–diffused Ti:$LiNbO_3$–waveguide lasers the fundamental phenomena of relaxation oscillations have been presented in detail in [21, 32]. The evolution of the pump– and signal intensity amplitudes as well as the space–dependent inversion and the repetition period as function of time have been calculated, explained and discussed (using a pre–version of the model and simulation techniques presented herein). As a representative example Fig. 4 again shows numerically calculated (left diagram) and experimentally observed (right diagram) relaxation oscillations of such a waveguide laser. The external pump power was

kept constant. At the beginning, when the amplitude of the signal is very low, the pump energy is used to build up and to increase the inversion. After a specific time, the onset time of the laser, sharp pulses appear. Their amplitudes decrease exponentially against the constant steady state output power. In general, a quasi quantitative agreement between calculated and experimentally observed data has been achieved: the calculated laser onset, the nearly exponential decay, the time–dependent repetition period (the distance between two neighboring signal pulses as function of time) as well as the steady–state signal amplitude are in a good accordance with the measurements.

5.2 Gain–Switched Laser Operation

Gain–switching is one method for generating and controlling short light pulses with large energies and a defined repetition frequency. Instead of pumping the laser continuously, the excitation process occurs with pump pulses of defined amplitude, width and frequency. Between two pump pulses the pump power is small. First of all, inversion has to be build up. After a certain time either a single large output spike or a sequence of more than one output spike can be generated. The number and the amplitudes of the signal pulses depend on the (external) pump pulses.

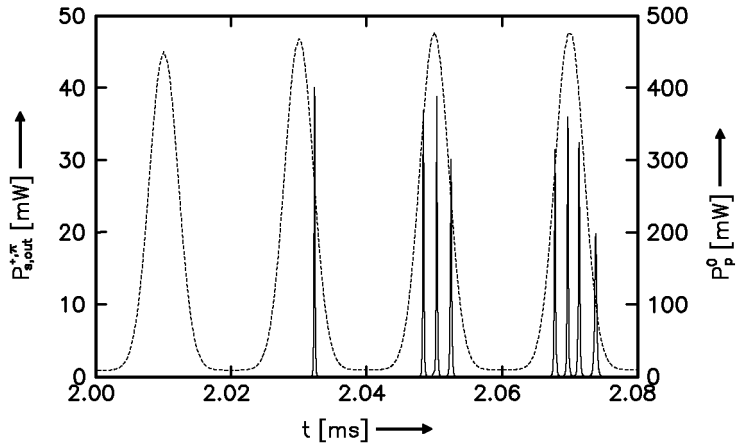

Fig. 5: Simulation of a gain–switched Er:Ti:$LiNbO_3$–waveguide laser.

Such a gain–switched laser operation has been simulated for an Er:Ti:$LiNbO_3$–waveguide laser based on the techniques presented above. During the first 2 ms the laser has been

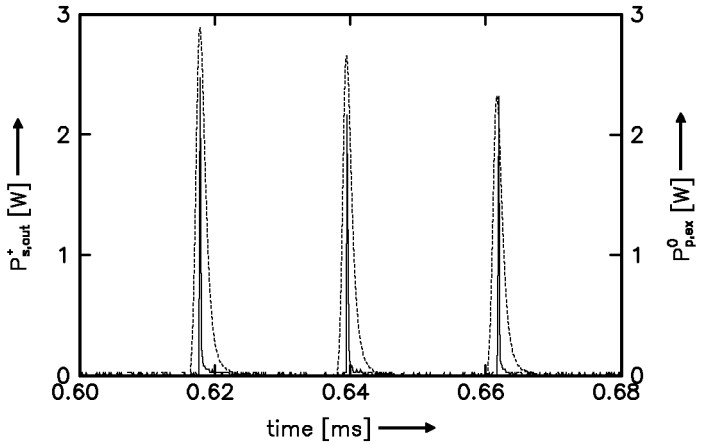

Fig. 6: Measured gain–switched operation of an Er:Ti:$LiNbO_3$–waveguide laser. Note that the experimental situation differs from the simulated one presented in Fig. 5. In the experiment the pump pulses were adaptively controlled in order to produce one single signal pulse only; the simulation demonstrates the possibility for generating sequences of signal pulses.

pumped with a constant pump power below the lasing threshold. For times $t > 2\,\mathrm{ms}$ Gaussian pulses with $3\,\mu s$ width and amplitudes 50 times higher than the constant value have additionally been superimposed to the constant pump power every $20\,\mu\mathrm{s}$. Fig. 5 shows the resulting output power together with the pump power within the resonator as a function of time. During the first pump pulse the inversion still is too low for laser operation. The first signal pulse appears at the end of the second pump pulse. Due to the decreasing pump and therefore due to the decreasing inversion further signal pulses are suppressed. During the third and the following pump pulses an irregular sequence of signal pulses with different amplitudes are generated.

In order to produce one signal pulse at each pump pulse the pump modulation function has to be adapted. Fig. 6 shows such a behaviour as it is experimentally observed. In the measurements presented the width and the amplitude of the pump pulses have been adapted so that for each pump pulse only one signal pulse appears. Nevertheless, during the first pump pulse a second signal pulse can be seen but strongly suppressed due to the decreasing pump pulse.

5.3 Q–Switched Laser Operation

Q–switching or giant pulsing is a another widely used technique for the generation of very short, very intense pulses at defined times [14]. The principle of this method is to build up a population inversion inside the laser cavity which is much larger than usual. This can be realized by decreasing the quality (Q) of the resonator or in other words by increasing the cavity losses e.g. by removing or blocking one of the feedback laser elements. After a certain time the losses are suddenly reduced; the quality of the laser is switched to a higher value. The result is that all the stored energy in form of the accumulated inversion dumps in only one (giant) single pulse.

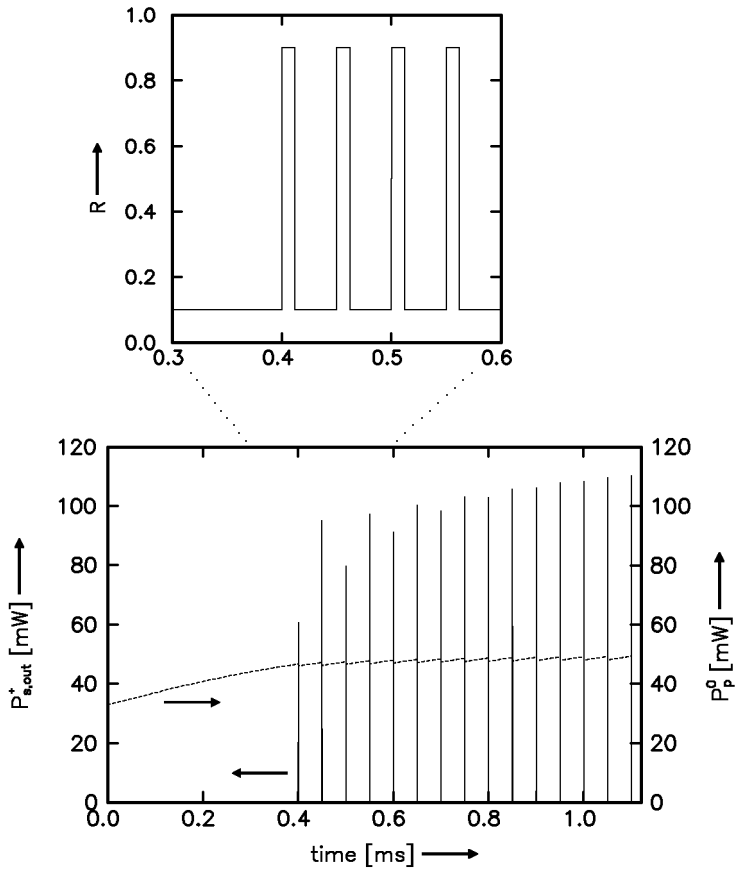

Fig. 7: Q–switched Er:Ti:$LiNbO_3$–waveguide laser. Left: Signal output power and pump power within the cavity as function of time. Right: Reflectivity of one of the two dielectric mirrors versus time. The calculations have been obtained using a typical parameter set [11].

In $LiNbO_3$ an erbium–doped Q–switched waveguide laser can be fabricated using a waveguide amplifier, an electro–optically switchable directional coupler and different dielectric mirrors at the waveguide endfaces [11]. By switching the light either in the bar or in the cross state of the coupler the quality of the resonator is changed. In one case the signal is reflected by a dielectric mirror (high reflectivity), in the other case by the waveguide endface (low reflectivity). In Fig. 7 the signal output power, the pump power within the resonator and the resulting reflectivity of such a laser are shown as computed using the model presented. A high reflectivity has been periodically adjusted (every 50 μs for 1.2 μs). After an inversion build up time of 0.4 ms the first signal pulse sets in. An experimental realization of Q–switching in Er:$LiNbO_3$–waveguide lasers is still under investigation.

5.4 Stochastical Pump Noise

In subsection 5.1 we have compared simulation and experimental results of relaxation oscillations resulting from a constant external pump input. There are some differences between the calculated and measured data (see Fig. 4), which are minor on the first glance. The decay of the pulse intensity is smooth in the simulation result while the measurement shows an irregular disturbance (shape fluctuation). Surely, a physicist's first idea for explaining this difference will be as follows: the assumption of constant external pump input is idealistic; in the real situation the input will be stochastically disturbed leading to the observed small irregular disturbance of the output signal. Indeed, as it can be seen in Fig. 4, the measurement shows that the pump input was not constant in time but that it looks like a constant one with additional stochastic noise with small amplitude. Consequently, we should try to reproduce the observed signal fluctuation by simulating a stochastically disturbed pump.

We construct a model for the perturbed pump input in which we stochastically repeat to add small deviations with Gaussian shape to the former constant p–value choosing amplitude and width of each pulse randomly equidistributed. Fig. 8 shows a typical result. The calculated signal shows characteristic shape fluctuations. This seems to confirm our guess that the noise in the pump input changes the decay of the signal pulses as it is observed. But, unfortunately, in some situations the measured signal output does not show any characteristic pulse decay at all (cf. Fig. 9). The question is, whether this can be an effect of pump noise, too? Or is it due to some other physical processes? If pump noise can effect such behaviour we should be able to observe this in simulation

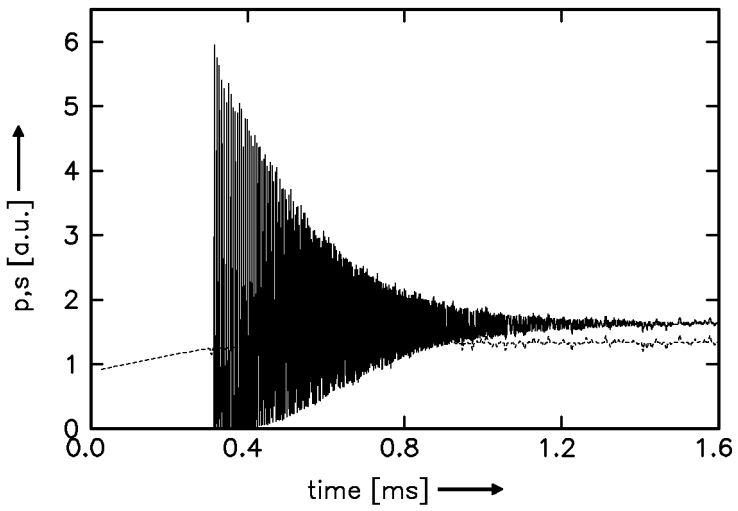

Fig. 8: Calculated relaxation oscillations of an Er:Ti:$LiNbO_3$–waveguide laser. The incident pump power has been stochastically disturbed.

calculations using the "right" model for the pump noise. Failing in this would lead to the assumption that in these cases processes are important which are not correctly represented in the actual model (e.g. spatial hole burning (frequency beating effect leading to standing wave patterns in the optical intensity) [14], optical damage (intensity induced refractive index change) [33], etc.). Up to now, this question is an open one. Some calculations allow to reproduce the effect but use irrealistically large noise amplitudes (see the middle diagram of Fig. 10). But the nonlinear nature of the process may lead to similar results for smaller amplitudes but a "better" noise model. However, this discussion is typical for the process of understanding physical phenomena using simulation calculations. First, the reliability of the numerical solution of the model equations allows a *direct comparison between model and experiment*, because the possibility of numerical artifacts need not be discussed simultaneously. Second, even the possible failure of a successful model in some situations allows the investigation and understanding of its reason.

Independently from the answer to the question asked a few lines above, modellers want to develop recipes to *guarantee* the decay of the signal pulses. This can be realized by a feedback of the signal output power to the external pump input power. Fig. 10 presents simulation results. The upper diagram shows the calculated relaxation oscillations for a constant pump input power leading to smooth behaviour as explained in section 5.1. In

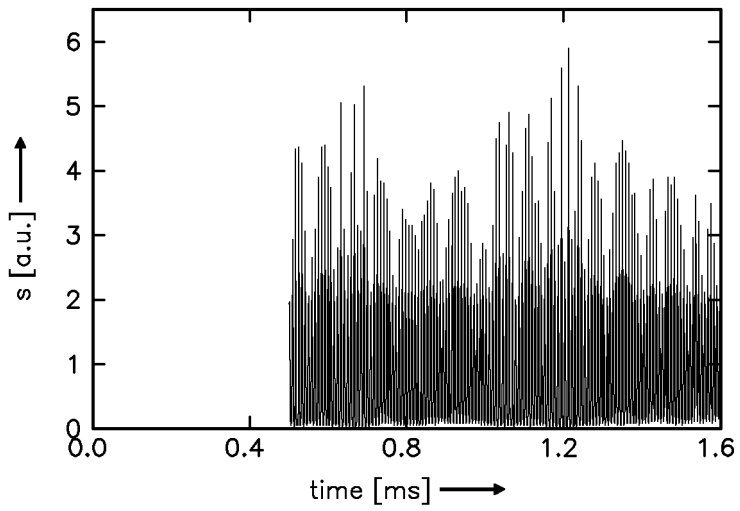

Fig. 9: Measurement of relaxation oscillations in an Er:Ti:$LiNbO_3$–waveguide laser. Instead of using a (nearly) constant pump power the signal output power is still fluctuating after 1.6 ms.

the middle diagram the pump input power has been disturbed stochastically as indicated by the dotted line resulting in a quasi–chaotic behaviour of the signal. Nevertheless, after 1.2 ms (which is 0.5 ms later than seen in the unperturbed case) a steady–state signal output is seen. In order to suppress the unwanted signal spikes a closed control loop is used. The pump power is controlled by "inverse backcoupling" of the difference of the signal output power s and the steady state value $\hat{s}$ wanted. Again, the presented model allows the simulation of this process. In particular the behaviour of s and p can be determined with respect to the strength of the backcoupling and $\hat{s}$. The lower diagram of Fig. 10 shows the result obtained for a typical parameter set. The uncorrelated spikes are damped leading to a behaviour similarly observed in experiments.

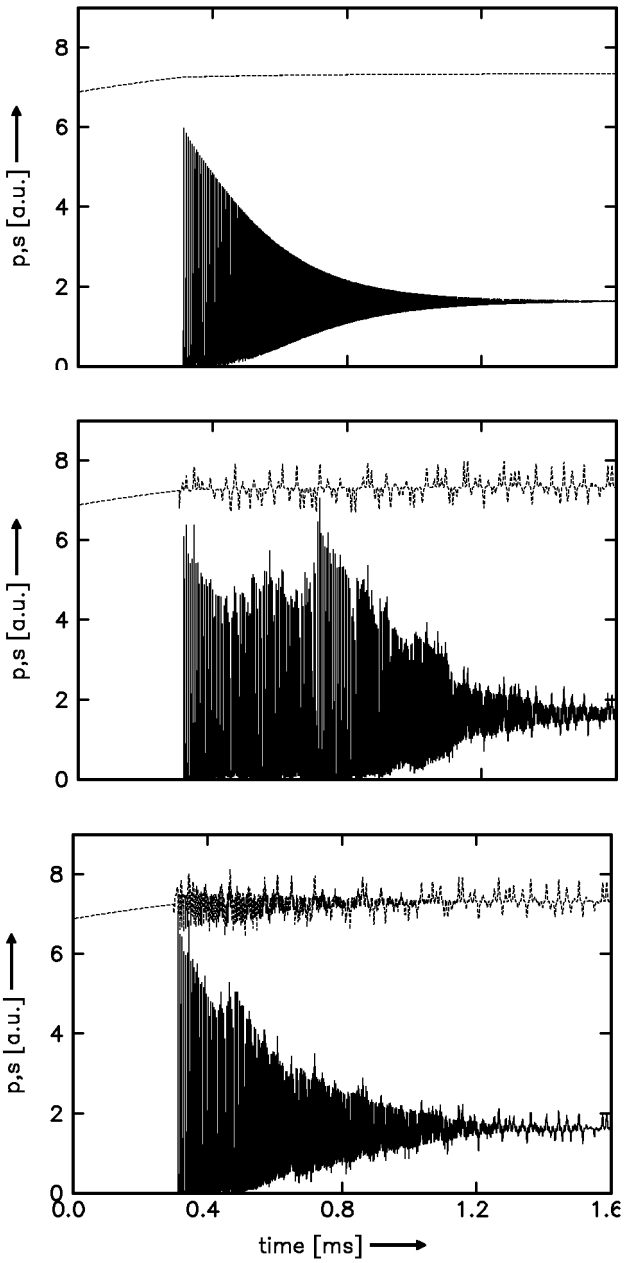

Fig. 10: Calculated results of relaxation oscillations in an Er:Ti:$LiNbO_3$–waveguide laser. The three diagrams show the behaviour of the signal output power as function of different pump input powers. In the upper diagram the pump power $P_{p,ex}$ was held to be constant in time, in the middle diagram $P_{p,ex}$ has been stochastically disturbed, which first leads to a quasi–chaotic behaviour for the signal output power. After 1.2 ms a steady state of fairly constant output power is achieved. The lower diagram shows the answer of the waveguide laser in which the (perturbed) pump power simultaneously has been coupled with the inverted signal power. It can be seen that the fluctuations are suppressed.

6 Conclusions

In the herein considered situation the technologically necessary calculations require reliable long term simulations of a complex dynamical behaviour. This demands a theory which is valid for the description of the processes considered and which, at least in principal, permits reliable simulations on the computers being available. Therefore, numerical algorithms have to be constructed which are appropriate for realizing these simulations efficiently and for controlling their reliability. In our case, the technology of the waveguide laser devices exploits the coupling between different "active" systems (light and matter) and therefore introduces a complex interplay between different processes (propagation and transition). We showed that this complexity demands cooperation between modelling, numerical analysis, algorithm construction, and experimental justification. We passed four steps: 1. construction of a fundamental model starting from accepted physical theories (Maxwell and rate equations) and recognizing this model to be numerically intractable, 2. reformulation via averaging resulting in a model with reduced complexity, 3. construction and implementation of adaptive, error controlling numerical algorithms leading to efficient and reliable simulations and paying attention to the sensitivity of the solution with respect to the model parameters, and 4. comparison with experimental observations and justification of the derived simulation techniques through showing it to be an instrument for quantitative analysis and prediction. Finally, we want to emphasize that we have not presented a *final* theory but that discussion and iteration of these four steps leads to a deeper understanding of the underlying physical processes (cf. section 5.4). In the context of *development* particularly, the evolution of this physical understanding is the main topic of modelling.

Acknowledgement

The authors gratefully acknowledge the support of this work by the European Union within the RACE–program (project R2013 EDIOLL (Erbium Doped Integrated Optical $LiNbO_3$ Lasers)). Special thanks to U. Rust and C. Deittert for fruitful discussions during the preparation of the manuscipt.

References

[1] Desurvire, E.: *Erbium–Doped fiber amplifiers: principles and applications*, John Wiley & Sons, Inc., New York (1994)

[2] Mears, R. J., Baker, S. R.: "Erbium fiber amplifiers and lasers" (tutorial review), Opt. and Quant. Electr., **24**, 517–538 (1992)

[3] Glass, A.: *Fiber optics*, Physics Today (1993)

[4] Bergano, N. S., Davidson, C. R., Homsey, G. M., Kalmus, D. J., Trischitta, P. R., Aspell, J., Gray, D. A., Maybach, R. L.: "9000 km, 5 Gb/s NRZ transmission experiment using 274 erbium–doped fiber amplifiers", in *Optical amplifiers and their applications technical digest*, (Optical Society of America, Washington, D. C.), **17**, PD–11 (1992)

[5] Imai, T., Muraki, M., Fukada, Y., Aiki, M., Ito, T.: "Over 10 000 km straight line transmission system experiment at 2.5 Gb/s using in–line optical amplifiers", in *Optical amplifiers and their applications technical digest*, (Optical Society of America, Washington, D. C.), **17**, PD–12 (1992)

[6] Kitagawa, T., Hattori, K., Shimizu, M., Ohmori, Y., Kobayashi, M.: "Guided–wave laser based on erbium–doped silica planar lightwave circuit", Electr. Lett., **27**, no. 4, 334–335 (1991)

[7] Brinkmann, R., Baumann, I., Dinand, M., Sohler, W., Suche, H.: "Erbium–doped single– and double–pass Ti:$LiNbO_3$ waveguide amplifiers", J. Quantum Electr., **30**, no. 10, 2356–2360 (1994)

[8] Brinkmann, R., Sohler, W., Suche, H.: "Continuous–wave erbium–diffused $LiNbO_3$ waveguide–laser", Electron. Lett., **27**, 415–416 (1991)

[9] Becker, P., Brinkmann, R., Dinand, M., Sohler, W., Suche, H.: "Er–diffused Ti:$LiNbO_3$ waveguide laser of 1563 and 1576 nm emission wavelengths", Appl. Phys. Lett., **61**, 1257–1259 (1992)

[10] Jackson, J. D.: *Classical Electrodynamics*, De Gruyter, Berlin (1981)

[11] Dinand, M.: *Modellierung erbiumdotierter integriert optischer Verstärker und Laser in $LiNbO_3$*, Dissertation Universität–GH Paderborn, Cuviller–Verlag Göttingen (1995)

[12] Kogelnik, H.: "Theory of dielectric waveguides", in Topics in Applied Physics, vol. 7, *Integrated Optics*, Ed.: Tamir, T., Springer Verlag, Berlin, Heidelberg, New York (1979)

[13] Courant, R., Hilbert, D.: *Methods of Mathematical Physics*, Volume II, John Wiley and Sons, New York, Chichester, Brisbane, Toronto, Singapore (1962)

[14] Siegman, A. E., *Lasers*, University Science Books, Mill Valley, California (1986)

[15] Desurvire, E.: "Study of the complex atomic susceptibility of erbium–doped fiber amplifiers", J. Lightw. Techn., **8**, no. 10, 1517–1527 (1990)

[16] Milonni, P. W., Eberly, J. H.: *Lasers*, New York: Oxford Science Publications (1985)

[17] Morkel, P. R., Laming, R. I.: " Theoretical modelling of erbium–doped fibre amplifiers with excited–state absorption", Opt. Lett. , **14**, 1062–1064 (1989)

[18] Desurvire, E., Simpson, J. R.: "Amplification of spontaneous emission in erbium–doped single–mode fibers", J. Lightw. Techn., **7**, no. 5, 835–845 (1989)

[19] Blixt, P., Nilsson, J., Jaskorzynska, B.: "Amplification reduction in fiber amplifiers due to up–conversion at Er^{3+} concentrations below 1000 ppm", Fib. Integr. Optics, **10**, 225–230 (1992)

[20] Dinand, M., Sohler, W.: "Theoretical modelling of optical amplification in Er–doped Ti:$LiNbO_3$–waveguides", J. Quantum Electr., **30**, no. 5, 1267–1276 (1994)

[21] Dinand, M., Schütte, Ch.: "Theoretical modelling of relaxation oscillations in Er–doped waveguide lasers", J. Lightw. Techn., **13**, no. 1, 14–23 (1995)

[22] Hairer, E., Wanner, G.: *Solving ordinary differential equations II, stiff and differential–algebraic problems*, Springer Verlag, Berlin, Heidelberg, New York, Tokyo (1980)

[23] Bornemann, F.: "An adaptive multilevel approach to parabolic equations I. General theory and 1d–implementation", Impact Comput. Sci. Engrg., **2**, 279–317 (1990)

[24] Schütte, Ch., Hohmann, A., Dinand, M.: "Numerical simulation of relaxation oscillations of waveguide lasers", Technical Report TR 93–14, Konrad–Zuse–Zentrum für Informationstechnik Berlin (ZIB), Berlin (1993)

[25] Deuflhard, P., Bornemann, W.: *Numerische Mathematik II – Integration gewöhnlicher Differentialgleichungen*, De Gruyter, Berlin (1994)

[26] Deuflhard, P., Hohmann, A.: *Numerical Analysis. A first course in scientific computation.*, De Gruyter, Berlin, New York (1995)

[27] Deuflhard, P.: "Uniqueness theorems for stiff ODE initial value problems", Proceedings 13th Biennial Conference on Numerical Analysis, 74–88, University of Dundee (1989)

[28] Hohmann, A., Wulff, C.: "Modular design of extrapolation codes", Technical Report TR 92–5, Konrad–Zuse–Zentrum für Informationstechnik Berlin (ZIB), Berlin (1992)

[29] Deuflhard, P.: *Order and stepsize control in extrapolation methods*, Numer. Math., **41**, 399–422 (1983)

[30] Zumbusch, G. W.: "Adaptive strategies in numerical quadrature", Preprint, Konrad–Zuse–Zentrum für Informationstechnik Berlin (ZIB), Berlin (in preparation)

[31] Hanna, D. C., Smart, R. G., Suni, P. J., Ferguson, A. I., Phillips, M. W.: "Measurement of fiber laser losses via relaxation oscillations", Opt. Com., **68**, no. 2, 128–132 (1988)

[32] Dinand, M., Schütte, Ch., Brinkmann, R., Sohler, W., Suche, H.: "Relaxation oscillations in Er–diffused Ti:$LiNbO_3$ waveguide lasers", Proc. 6th Europ. Conf. Integrated Optics (Neuchâtel, Schweiz), 3–20 (1993)

[33] Glass, A. M.: "The photorefractive effect", Optical Engineering, **17**, 470–479 (1978)